CHAPTER - 6

CORROSION INHIBITING EFFECT OF BIS-ISOXAZOLES, PYRAZOLES, PYRIMIDINES FOR MILD STEEL IN 1M H_2SO_4

6.1 INTRODUCTION

Bis-heterocyclic compounds are gaining increased interest in the recent past as the dimeric analogues have proven to have better and potent biological activity than the corresponding monomer. Bis-derivatives represent an important class of well-studied heterocycles. The interest in this kind of heterocycles has spread from the early dye chemistry to modern drug design, biodiagnostics, electronic and optoelectronic devices, conductivity-based sensors and self-assembled superstructures. Bis-heterocylces have been developed for different purposes in the pharmaceutical field and have been tested as potential antitumor, antiviral, antibiotic, antiglaucoma drugs, as inhibitors of platelet aggregation[1-5] and are of considerable interest as potential biologically active compounds and pharmaceuticals. Bis-heterocylces have gained importance as excellent inhibitors for corrosion of mild steel and its alloys in acidic solution[6] due to their characteristic structure and high inhibition performance.

In continuation of our work on the acid corrosion inhibitors, some bis-heterocyclic derivatives have been synthesized and evaluated as corrosion inhibitors for mild steel corrosion in H_2SO_4 solution. The inhibitive performance of the synthesized bis-compounds was studied by weight loss measurements, electrochemical impedance spectroscopy (EIS) and potentiodynamic polarization analysis. The effect of temperature (303 - 333 K) on the corrosion and inhibition process were thoroughly assessed and discussed. Thermodynamic parameters governing the adsorption processes were also calculated and computed. The mild steel surface after treatment in the absence and presence of the inhibitors, were analysed by FTIR, SEM-EDS, XRD and AFM. A probable inhibitive mechanism was also proposed to explain the results. Quantum chemical study using density functional theory (DFT) at the B3LYP/6-31G(d,p) method dwas further employed to compare the inhibitive effect of the bis-compounds with conventional methods.

6.2 EXPERIMENTAL WORK

6.2.1 Synthesis of inhibitors

(i) Synthesis of bis-chalcones (I_{a-c})

Acetophenone/3-acetyl pyridine/3-acetyl-2,5-dimethyl thiophene (0.029 mol) (1) terephthaldehyde (2 g, 0.014 mol) (2), 95% EtOH (20 ml) and NaOH (5 g in 10 ml EtOH) were taken in a 100 ml conical flask. The mixture was irradiated by an ultrasonic generator in a water bath at 30 - 35°C for 5 minutes. The solid product so formed was diluted with water and neutralized with 2N HCl (3 ml) then it was filtered, washed well with cold water and purified by chromatography using CH_2Cl_2/n-hexane (1:1)[7].

(ii) Synthesis of bis-pyrimidine derivatives[8] (II_{a-f})

A mixture of bis-chalcone (0.01 mol), thiourea/urea (0.02 mol) were dissolved in ethanolic sodium hydroxide and refluxed for 24 hours. The precipitate obtained was filtered, washed and recrystallized from ethanol.

(iii) Synthesis of bis-azole derivatives[8] (II_{g-l})

A mixture of bis-chalcone (0.01 mol), hydrazine hydrate/hydroxylamine hydrochloride (0.02 mol) and glacial acetic acid (10 ml) in ethanol (25 ml) was refluxed for 24 hours. The mixture was concentrated by distilling out the solvent under reduced pressure and poured into ice water. The precipitate obtained was filtered, washed and recrystallized from ethanol[9]. The reactions are presented in **Scheme 6.1**.

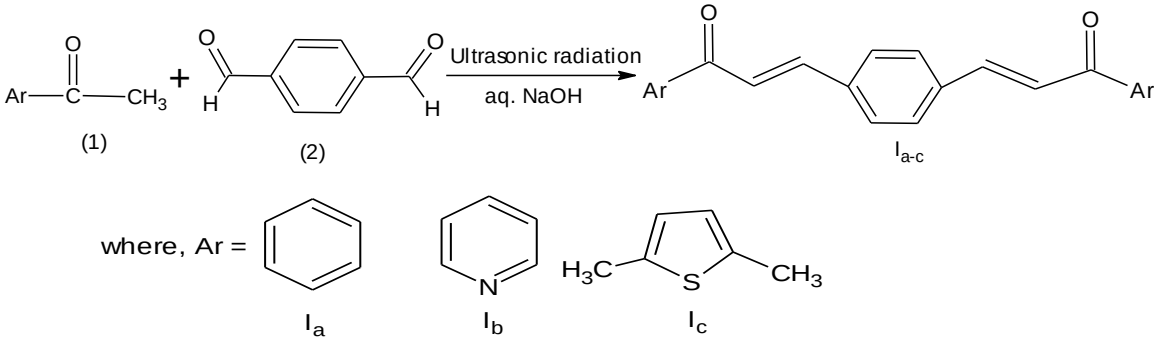

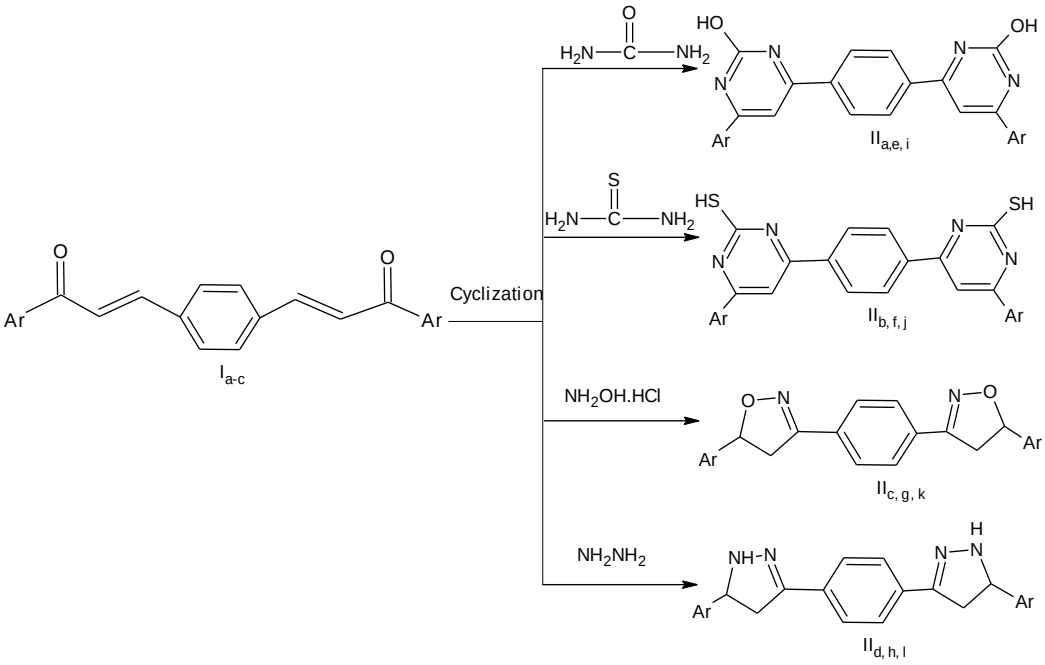

Scheme 6.1

The synthesized compounds were characterized by FTIR spectra using IR Affinity 1 spectrometer (Shimadzu)

Code no.	Abbreviated name	Code no.	Abbreviated name	Code no.	Abbreviated name
II_a	BPH	II_e	BPPH	II_i	DTPH
II_b	BPT	II_f	BPPT	II_j	DTPT
II_c	BPO	II_g	BPPO	II_k	DTPO
II_d	BPP	II_h	BPPP	II_l	DTPP

6.2.2 Evaluation of inhibition efficiency of bis-heterocyclic derivatives

Non-electrochemical and electrochemical corrosion measurements were carried out, as reported in the previous chapters 3, 4 and 5 of this thesis. 1M H_2SO_4 was prepared by dilution of analytical grade H_2SO_4 with distilled water. The concentration range of inhibitors used were 0.05 mM, 0.1 mM, 0.25 mM, 0.35 mM, 0.5 mM and 1 mM in 1M sulphuric acid. Surface morphology studies like FTIR, SEM-EDS, XRD and AFM were also carried out. Quantum chemical calculations were performed using Density functional theory method at B3LYP/6-31G(d,p) basis set.

6.3 RESULTS AND DISCUSSION

The inhibitors were synthesized by condensing terephthaldehyde with acetophenone/3-acetyl pyridine/3-acetyl-2,5-dimethyl thiophene *via* ultrasonic radiation to get bis-chalcones. The obtained bis-chalcones were cyclized with urea/thiourea to get pyrimidine derivatives and with hydroxylamine hydrochloride/hydrazine hydrate to get azole derivatives. The molecular structure of the synthesised compounds and the physical constants are presented in Tables 6.1. The structure of the synthesized bis-pyrimidines, bis-isoxazoles and bis-pyrazoles were confirmed by IR spectra [4000 - 400 cm^{-1}]. The FTIR spectral data are presented in Table 6.2 [Figs. 6.1 - 6.12].

In bis-pyrimidine derivatives bands characteristic of >C=N, -OH, -SH stretching frequencies were observed at 1593.27 - 1611.59 cm^{-1}, 3427.65 - 3435.37 cm^{-1} and 2196 - 2353.26 cm^{-1} respectively. Similarly for the bis-pyrazoles and bis-isoxazoles bands characteristic of >C=N-, -NH, >C-O-C< groups were observed at 1619.31 - 1651.14 cm^{-1}, 3212.58 - 3347.60 cm^{-1} and 1353.12 - 1367.59 cm^{-1}. The bands around 1519.97 - 1572.05 cm^{-1}, 1406.17 - 1461.14 cm^{-1} are attributed to >C=C< stretching frequencies of the aromatic ring.

6.3.1 Corrosion monitoring techniques

6.3.1.1 Non-Electrochemical methods

(i) Gravimetric measurements

A number of mechanistic studies on the anodic dissolution of iron in acidic sulphate solutions have been undertaken and the hydroxy accelerated mechanism proposed initially by **Bockris** and **Drazic**[9] and reported by **Oguzie**[10] has gained wide acceptance:

$$Fe + H_2O \Longleftrightarrow (FeOH)_{ads} + H^+ + e^- \longrightarrow \quad 6.1$$

$$(FeOH)_{ads} \longrightarrow (FeOH)^+ + e^- \longrightarrow \quad 6.2$$

$$(FeOH)^+ + H^+ \Longleftrightarrow Fe^{2+} + H_2O \longrightarrow \quad 6.3$$

As a consequence of these reactions, including the high solubility of the corrosion products, the metal losses weight in the solution. Corrosion inhibition is initiated by the displacement of adsorbed water molecules by inhibitor species leading to the specific adsorption of the inhibitor on the metal surface[11].

In order to evaluate the effect of inhibitor concentration on inhibition efficiency, weight loss experiments were performed on mild steel specimens for 3 hours immersion time at 303 K. The weight loss parameters such as corrosion rate (CR), inhibition efficiency (%) and corresponding surface coverage (θ) are given in Table 6.3. It is apparent from Table 6.3 that inhibition efficiency increases with increase in inhibitor concentration. The increase in inhibition performance with concentration can be attributed to an increase in the number of inhibitor molecules adsorbed on the metal surface, which separate the mild steel from the acid solution, resulting in the retardation of metal dissolution[12].

From Table 6.3, it is clear that the order of inhibition efficiency of the synthesized bis-derivatives are as follows: Thiophene derivatives: DTPT > DTPH > DTPP > DTPO; Pyridine derivatives: BPPT > BPPH > BPPP > BPPO; Benzene derivatives: BPT > BPH > BPP > BPO. Among the series, DTPT, BPPT and BPT showed the maximum inhibition efficiency of 99.03%, 93.05% and 84.02% respectively at 1 mM. This may be due to the presence of mercapto substituent in the organic structures which makes the formation of dπ-dπ bond resulting from overlap of 3d electrons from Fe atom to the 3d vacant orbital of the sulphur atom possible[13], which enhances the inhibition efficiency of the compounds on the metal surface. Indeed, the protective properties of all the synthesized bis-derivatives are probably due to the ineteraction between π-electrons and heteroatoms (O, N & S) with positively charged steel surface[14]. Moreover, the corrosion rate values are also seen to decrease with increase in concentration of bis-derivatives as shown in Table 6.3. This actually confirms that the addition of even a very small amount of bis-derivatives to the acid solution retards the corrosion rate of the metal and the extent of retardation is concentration and temperature dependent.

(ii) Influence of temperature

For most chemical reactions, the reaction rate increases with increasing temperature. Temperature affects the corrosion rate of metals in electrolytes primarily through its effect on factors which control the diffusion rate of oxygen. The corrosion of iron and steel is an example of this, because temperature affects the corrosion rate by virtue of its effect on the oxygen solubility and oxygen diffusion coefficient. As temperature increases the diffusion coefficient of oxygen also increases which tends to

increases the corrosion rate. However as temperature is increased, oxygen solubility in aqueous solution decreases until at the boiling point all oxygen is removed, this factor tends to decreases the corrosion rate. The net effect for mild steel is that, the corrosion rate approximately doubles for a temperature rise of 313 K up to a maximum temperature of about 343 K, and then the corrosion rate falls off in an open system because the decrease in oxygen solubility becomes the most important factor. In a closed system, where oxygen cannot escape, the corrosion rate continues to increase indefinitely with temperature until all the oxygen is consumed[15].

The effect of temperature on the corrosion inhibition performance of bis-derivatives on mild steel in 1M H_2SO_4 have been investigated by weight loss measurements in the temperature range 303 - 333 K in the absence and presence of inhibitors ($II_{a\text{-}l}$) at optimum concentration of 1 mM. The corresponding data are shown in Table 6.4. Table 6.4 shows the value of corrosion rate, surface coverage and inhibition efficiency obtained from weight loss measurements at various temperatures. It is apparent from the data in Table 6.4 that the bis-derivatives get desorbed on the mild steel surface at all temperatures studied and corrosion rate increases with increase in temperature in inhibited solutions.

A decrease in percentage inhibition with temperature has been reported by **Olivares *et al.*,**[16] due to a reduction in stability of the adsorbed film at higher temperature: as temperature increases, Gibbs free energy and enthalpy rises to a higher value, so that some of the chemical bonds joining the molecules on to the metallic surface are impaired and the stability of the film reduces. This is likely to result in desorption of the inhibitor film from the metal surface and a shift in the position of the inhibitor-metal interfacial equilibrium.

(iii) Activation parameters for corrosion processes

In order to calculate the activation energy (E_a) for the corrosion process, Arrhenius equation is used

$$CR = A \exp\left(-\frac{E_a}{RT}\right) \longrightarrow 6.4$$

where CR is the corrosion rate, A is the Arrhenius pre-exponential factor, E_a is the activation energy for the corrosion process, R is the molar gas constant

(8.314 J K^{-1} mol^{-1}) and T is the absolute temperature. The apparent activation energies (E_a) at optimum concentration (1 mM) of the inhibitors were determined by linear regression between log CR vs. 1000/T and are represented in Fig. 6.13. Plot of log CR vs. 1000/T gave straight lines with slope $\left(-\frac{E_a}{2.303R}\right)$ and intercept A. The linear regression coefficients were close to unity for all the inhibitors ($II_{a\text{-}l}$) analysed. Arrhenius law predicts that corrosion rate increases with the temperatue and E_a may vary with temperature in accordance with equation 6.4. Inspection of Table 6.5 showed that the value of E_a for the uninhibited solution was found to be 48.45 kJ mol^{-1} whereas in the presence of inhibitors it is 58.79 - 80.22 kJ mol^{-1}. It is clear that activation energy is higher in inhibited solution than in uninhibited solution. The increase in the apparent activation energy in the inhibited solution suggests physical adsorption of the inhibitors on the mild steel surface. The increase in activation energy can also be attributed to an appreciable decrease in the adsorption of the inhibitor on the mild steel surface with increase in temperature. As adsorption decreases, more desorption of inhibitor molecules occur because these two opposite processes are in equilibrium. Due to more desorption of inhibitor molecules at higher temperatures the greater surface area of mild steel comes in contact with aggressive environment resulting in increased corrosion rates with increase in temperature[17]. The very high activation energy in the presence of the inhibitor may be due to the physical adsorption of the inhibitor species on the mild steel surface. This type of inhibitor retards corrosion at ordinary temperatures but inhibition is diminished at elevated temperature[18]. Thus these inhibitors perform well at room temperatures.

Fig. 6.14 shows the plot of log CR/T vs. 1000/T for the corrosion of mild steel in the absence and presence of inhibitors ($II_{a\text{-}l}$) in 1M H_2SO_4. In order to calculate the activation parameters like ΔH^o and ΔS^o for the corrosion process, transition state equation[19] was used

$$CR = \frac{RT}{Nh}\exp\left(\frac{\Delta S^o}{R}\right)\exp\left(-\frac{\Delta H^o}{RT}\right) \longrightarrow 6.5$$

where CR is the corrosion rate, R is the molar gas constant, T is the absolute temperature, h is Planck's constant, N is Avogadro's number, ΔH^o and ΔS^o are the enthalpy and entropy of activations. Plot of log CR/T vs. 1000/T gave straight line with slope ($-\Delta H^o/2.303R$) and intercept [log(R/Nh) + ($\Delta S^0/2.303R$)] from which the values of ΔH^o

and ΔS^{o} were computed and listed in Table 6.5. Inspection of these data revealed that the enthalpy of activation for the dissolution reaction of mild steel in 1M H_2SO_4 in the presence of all inhibitors (II_{a-l}) is higher (56.15 - 77.58 kJ mol^{-1}) than that in the absence of the inhibitor (45.81 kJ mol^{-1}). Positive values of enthalpy of activation (ΔH^{o}) in the absence and presence of inhibitors reflect the endothermic nature of the mild steel dissolution process meaning that dissolution of steel is difficult. It is evident from Table 6.5 that the value of ΔH^{o} increased in the presence of the inhibitors compared to the uninhibited solution indicating higher protection efficiency. This may be attributed to the presence of energy barrier for the reaction, hence the process of adsorption of the inhibitor leads to rise in enthalpy of the corrosion process.

The value of ΔH^{o} and E_a are nearly the same and are higher in the presence of the inhibitors. This indicates that the energy barrier of the corrosion reaction increased in the presence of the inhibitor without changing the mechanism of dissolution. The value of E_a is found to be larger than the corresponding ΔH^{o} value indicating that the corrosion process must involve a gaseous reaction, simply the hydrogen evolution reaction, associated with a decrease in the total reaction volume[20, 21]. Moreover, the difference in the value of E_a-ΔH^{o} is found to be 2.6 kJ mol^{-1}, which is approximately equal to the average value of RT (2.63 kJ mol^{-1}). This indicates that the corrosion process is a unimolecular reaction as it is characterized by the following equation:

$$E_a - \Delta H^{\circ} = RT \longrightarrow 6.6$$

On the other hand, the negative value of ΔS^{o} in the absence and presence of inhibitors indicates that the formation of the activated complex in the rate determining step represents an association rather than a dissociation step, meaning that a decrease in disorder takes place during the course of the transition from reactants to acitvated complex[22].

(iv) Adsorption isotherm

An organic compound may be considered efficient and a successful inhibitor of acid corrosion if it is able to get adsorbed on the metal surface and this involves the replacement of water molecules at the corroding interface. Assuming that the metal is corroding uniformly, the corrosion rate of the acid in the absence of the inhibitor is

representative of the total number of available corroding sites. Therefore, the corrosion rate in the presence of the inhibitor may be taken as an representative of the number of potentially corroding sites that remain after blockage due to inhibitor adsorption[16].

Therefore, a direct relationship between inhibition efficiency (% IE) and the degree of surface coverage (θ) [% IE = 100 x θ] may be assumed for the different concentrations of the inhibitor. The degree of surface coverage (θ) for the different concentrations of bis-derivatives have been evaluated from the weight loss measurements in 1M H_2SO_4 at 303 K for 3 hours of immersion period. The data were tested graphically by fitting to various adsorption isotherms including Temkin, Flory-Huggin and Langmuir adsorption isotherms (Figs. 6.15 - 6.17). The correlation coefficient (R^2) was used to determine the best fit isotherm, which was obtained for Langmuir (Table 6.6). According to this isotherm, θ is related to the inhibitor concentraion by the following equation[23].

$$\frac{C}{\theta} = \frac{1}{K_{ads}} + C \qquad \longrightarrow \quad 6.7$$

where θ is the surface coverage, C is the concentration of inhibitor used in the corrosive medium, K_{ads} is the equilibrium constant of adsorption process. A straight line was obtained by plotting of C/θ vs. C with the R^2 value almost unity (Table 6.7) at 303 K, (Fig. 6.17), suggesting that the Langmuir adsorption isotherm model provides the best description of the adsorption behaviour. The K_{ads} value may be taken as a measure of the strength of the adsorption froces between the inhibitor molecules and the metal surface[24]. The relatively high values of the adsorption equilibrium constant for the inhibitors (BPT, BPPT, DTPT) reflect the high adsorption ability of these molecules on mild steel surface. The adsorption equilibrium constant K_{ads} is related to the standard free energy ΔG°_{ads} by the following equation 6.8.

$$K_{ads} = \frac{1}{55.5} \exp \frac{\Delta G^{\circ}_{ads}}{RT} \qquad \longrightarrow \quad 6.8$$

where 55.5 represent the molar concentration of water in solution (mol L^{-1}), R is the molar gas constant and T is the absolute temperature. Calculated values of free energy are also presented in Table 6.7. The values ranged from -14.56 to -23.10 kJ mol^{-1} and are within the range expected for the transfer of charge from the inhibitor to the metal surface. The negative values of standard free energy of adsorption indicate that spontaneous adsorption of the molecules on mild steel surface and also the strong

interaction between inhibitor molecules and the metal surface. Generally, values of ΔG°_{ads} up to -20 kJ mol^{-1} signify physisorpion, the inhibitor acts due to electrostatic interactions between the charged molecules and the charged metal, while values around -40 kJ mol^{-1} or less are associated with chemisorption as a result of sharing or transfer of electrons from the organic molecules to the metal surface to form a coordinate type of bond. The values obtained in this study (Table 6.7) support the mechanism of physical adsorption[25].

(v) Thermodynamic parameters

The enthalpy of adsorption was calculated from the Gibbs-Helmholtz equation:

$$\frac{\partial(\Delta G^{\circ}_{ads}/T)}{\partial T} = \frac{-\Delta H^{\circ}_{ads}}{T^2} \longrightarrow 6.9$$

This equation can be arranged to give

$$\frac{\Delta G^{\circ}_{ads}}{T} = \frac{\Delta H^{\circ}_{ads}}{T} + K \longrightarrow 6.10$$

The variation of ΔG°_{ads} /T with 1/T gives a straight line with slope equal to ΔH°_{ads} (Fig. 6.18). It can be viewed from the figure that ΔG°_{ads} /T decreases with 1/T in a linear manner. The calculated values are shown in Table 6.8.

The negative sign of ΔH°_{ads} in H_2SO_4 solution indicates that the adsorption of inhibitor molecule is an exothermic process. Generally, an exothermic adsorption process signifies either physisorption or chemisorption, while endothermic process is recognized as chemisorption[26].

The adsorption of heat can also be calculated according to the Van't Hoff equation (6.11)[27]

$$\ln K = -\frac{\Delta H^{\circ}_{ads}}{RT} + \text{constant} \longrightarrow 6.11$$

Fig. 6.19 shows the plot of ln K_{ads} vs. 1/T for mild steel dissolution in 1M H_2SO_4 in the presence of bis-derivatives which gives straight lines with slope ($-\Delta H^{\circ}_{ads}$ /2.303R) and intercept (ΔS°_{ads} /R + ln 1/55.5). The calculated values of ΔH°_{ads} using the Van't Hoff equation are same as that obtained for Gibb's Helmholtz equation for 1M H_2SO_4, (Table 6.8) confirming exothermic behaviour of the adsoption of bis-derivatives on the steel surface.

The values of ΔS°_{ads} in Table 6.8, is positive in H_2SO_4 solution. This could be explained in the following way: the adsorption of bis-derivatives from the aqueous solution can be regarded as quasi substitution process between the organic compound in the aqueous phase and water molecules at the mild steel surface[28]. In this situation, the adsorption of bis-derivatives is accompanied by desorption of water molecules from the surface. Thus the adsorption of inhibitor is believed to be exothermic and associated with decrease in entropy of the solute, the opposite is true for solvent. Since, the thermodynamic values obtained are the algebraic sum of adsorption of organic inhibitor molecule and desorption of water molecules[29]. Therefore, gain in entropy is attributed to increase in solvent entropy. It means that in H_2SO_4 solution, driving force for the adsorption of the adsorbate is the increase in entropy rather than the decrease in enthalpy.

6.3.1.2 Atomic absorption spectrophotometric studies

The inhibition efficiency (%) of the bis-compounds DTPT, BPPT and BPT was calculated from the percentage of Fe dissolved obtained from AAS and the data are presented in Table 6.9. The inhibition efficiency (%) obtained by this technique was found to be in good agreement with that obtained from the conventional weight loss method.

6.3.2 Electrochemical measurements

6.3.2.1 Electrochemical impedance spectroscopy

Impedance measurement is a veritable tool and has been widely used in investigating the corrosion inhibition processes. It provides information on both the resistive and capacitive behaviour at interface and makes it possible to evaluate the performance of the tested compounds as possible inhibitors against metals.

Electrochemical impedance behaviour of mild steel corrosion in 1M H_2SO_4 solutions in the absence and presence of optimum concentration of inhibitors at 303 K are shown in Figs. 6.20 a-l. From the Nyquist plot, depressed semicircles can be observed in which diameter of semicircle increases with increase in inhibitor concentrations, which indicates that the corrosion of mild steel is mainly controlled by a charge transfer process[30]. Nyquist plots show a single semicircle capacitive loop in the higher frequency (HF) region and a very small inductive loop in the lower frequency (LF) region. The

generation of HF capacitive loop may be due to electron transfer reaction and time constant of the electrical double layer and to the surface non-homogeneity of structural or interfacial origin such as those found in adsorption processes. The LF inductive loop may be attributed to the relaxation process obtained by the adsorbed species like $SO_{4\,ads}^{2-}$ and H_{ads}^{+} on the electrode surface.

Deviation of perfect circular shape is often referred to the frequency dispersion of interfacial impedance. This anomalous behavior is generally attributed to the inhomogeneity of the metal surface arising from surface roughness or interfacial phenomena[31,32]. The obtained semicircles cut the real axis at higher and lower frequencies. The intercept corresponds to R_s at the higher frequency end and $R_s + R_{ct}$ at the lower frequency end, where R_{ct} is the difference between these two values[33]. Double layer capacitance (C_{dl}), is obtained from the frequency at which the imaginary part of the impedance is maximum, ($-Z_{i\ max}$) and C_{dl} values are calculated from the following equation

$$C_{dl} = \frac{1}{2\pi\, R_{ct}\, f(-Z_i max)} \qquad \longrightarrow \quad 6.12$$

where $f(-Z_i\ \max)$ is the frequency at which the imaginary part of the impedance is a maximum. R_{ct} and C_{dl} derived from the impedance measurements are shown as a function of inhibitor concentrations. The interpretation of Nyquist plots (Figs. 6.20 a-l) allow to determine the electrochemical parameters of the steel electrode and to acquire information about the corrosion process and mechanism. The values of impedance parameters namely charge transfer resistance (R_{ct}), double layer capacitance values (C_{dl}) and calculated inhibition efficiencies (%) are reported in Table 6.10. Analysis of the data presented in Table 6.10 indicates that the magnitude of R_{ct} value increased, while that of C_{dl} values decreased with the addition of inhibitors to 1M H_2SO_4 medium at optimum concentration of inhibitors. The decrease in C_{dl} values results from the adsorption of the inhibitor molecules at the metal surface. The double layer between the charged metal surface and the solution is considered as an electrical capacitor. The adsorption of inhibitors on the mild steel surface decreases its electrical capacity as they displace the water molecules and other ions originally adsorbed on the surface leading to the formation of a protective adsorption layer on the electrode surface which increases the

thickness of the electrical double layer. The thickness of this protective layer (d) is related to C_{dl} in accordance with Helmholtz model, given by the following equation[34]

$$C_{dl} = \frac{\varepsilon\varepsilon_0 A}{d} \longrightarrow 6.13$$

where ε is the dielectric constant of the medium and ε_o is the permittivity of free space (8.854×10^{-14} F cm^{-1}) and A is the effective surface area of the electrode and d is the thickness of the interfacial layer. Since adsorption of an organic inhibitor on a metal surface involves the replacement of water molecules pre adsorbed on the surface, the smaller dielectric constants of organics compared to water as well as the increased thickness of the double layer due to inhibitor adsorption act simultaneously to reduce the interfacial capacitance. This provides experimental evidence of adsorption of bis-derivatives on the corroding mild steel surface. The adsorbed inhibitor, depending on its specific properties, can influence the corrosion reaction by either geometric blocking of the electrode surface, thereby restricting the access of corrosive species or transfer of corrosion products away from it, or by blocking and deactivating the active reaction sites on the electrode.

6.3.2.2 Potentiodynamic polarization measurements

Polarization measurements were carried out in order to gain knowledge concerning the kinetics of the cathodic and anodic reactions. The effect of addition of inhibitors on the anodic and cathodic polarization curves for mild steel in 1M H_2SO_4 solution was studied and the polarization curves are shown in Figs. 6.21 a-l at 303 K. The values of the cathodic (b_c) and anodic (b_a) Tafel slopes were calculated from the linear region of the polarization curves. The corrosion current density (I_{corr}) was determined from the intersection of the anodic and cathodic curves with the open circuit corrosion potential (E_{corr}). The corrosion parameters such as corrosion potential (E_{corr}), anodic Tafel slope (b_a), cathodic Tafel slope (b_c), corrosion current density (I_{corr}) and percentage inhibition efficiency (%) obtained from these curves are given in Table 6.11. It is evident from the Table 6.11 that the values of b_c changed with increasing inhibitor concentration, indicating the influence of the compounds on the kinetics of hydrogen evolution. The shift in anodic Tafel slope b_a may be due to the sulphate ions/or inhibitor molecules adsorbed onto the steel surface. Moreover, all the studied inhibitors may act as adsorption

inhibitors due to the presence of some active sites and hetero-atoms. Being adsorbed on the metal surface, the inhibitors control the anodic and cathodic reactions during corrosion processes and its corrosion inhibition efficiency is directly proportional to the amount of adsorbed inhibitor. The functional group and the structure of the inhibitor play important roles during the adsorption processes.

The results in Table 6.11 reveal that the addition of bis-derivatives at the studied concentrations decreased the anodic and cathodic current densities and resulted in significant decline in corrosion current densities and an increase in inhibition efficiency, confirming the presence of a protective film of inhibitor molecules on the mild steel surface[35]. The cathodic Tafel constant (b_c) relating to the polarization of mild steel in 1M H_2SO_4 is equal to 113 mV dec^{-1}. As reported in the literature[36], this value indicates, in general, that the reduction reaction of hydrogen on iron takes place according to the mechanism of **Volmer-Heyrovsky** reaction.

$$H^+_{ads} + e^- \longrightarrow H_{ads} \longrightarrow \quad 6.14$$

$$H_{ads} + H^+ + e^- \longrightarrow H_2 \longrightarrow \quad 6.15$$

In Tafel slopes, the b_c values changed after the addition of inhibitors, but this necessarily does not result from a modification of the reaction mechanism[37]. Indeed, when the coverage rate increases with increasing inhibitor concentration, the electrode active surface is reduced and the adsorbed film can have an ohmic behaviour, which appears by an increase in the b_c value[38].

If the displacement in E_{corr} in presence of inhibitor is more than ±85 mV/SCE relating to E_{corr} of the blank, the inhibitor may be considered as a cathodic or anodic type[39, 40.] In the present study the maximum displacement is approximately equal to 8.2 to 61.4 mV, which confirmed that the bis-derivatives acted as a mixed type inhibitors. It is obvious from Figs. 6.21 a-l that, the minor shift of E_{corr} values towards positive direction suggests the predominant anodic control over the reaction[41].

6.3.3 Surface characterization

6.3.3.1 FTIR analysis of mild steel plate

Figs. 6.22 - 6.24 shows the FTIR spectra of compounds DTPT, BPPT and BPT immersed in 1M H_2SO_4 solution for a period of 3 hours with optimum concentration of

inhibitors. In comparison to the FTIR spectra of the inhibitors (Table 6.2), it is evident that >C=N, -SH, stretching frequencies have shifted to a considerable extent in DTPT, BPPT and BPT. Stretching frequency of >C=N- has shifted from 1603.88 cm^{-1}, 1600.02 cm^{-1}, 1611.59 cm^{-1} to 1610.85 cm^{-1}, 1664.64 cm^{-1} and 1663.68 cm^{-1} respectively. Similarly, stretching frequency of SH shifted from 2353.26 cm^{-1}, 2312.75 cm^{-1}, 2196.05 cm^{-1} to 2346.51 cm^{-1}, 2304.07 cm^{-1} and 2301.18 cm^{-1}, confirming that these electron centres are involved in the adsorption process. Moreover, >C=C< stretching frequencies of the aromatic ring have shifted to considerable extent confirming the active participation of >C=C< in the adsorption process.

6.3.3.2 Scanning electron microscope-Energy dispersive X-ray spectroscopy (SEM-EDS)

SEM and EDS experiments were carried out in order to verify if the investigated compounds are in fact adsorbed on mild steel surface or just peeled off from the surface. SEM images are indicative of the changes that accompany both corrosion and protection of the mild steel surface. Figs. 6.25 - 6.27 show the SEM micrographs of the mild steel surface exposed to 1M H_2SO_4 without and with optimum concentration (1 mM) of inhibitors after 3 hours immersion time. Fig. 6.25 represents the mild steel surface in the absence of inhibitors in which the steel specimen is strongly damaged due to the formation of corrosion products. Figs. 6.26 and 6.27 shows the SEM micrographs of the mild steel surface after immersion in 1M H_2SO_4 containing 1 mM concentration of the investigated inhibitors DTPT and BPPT. From these images it is obvious that no pits and cracks are observed in the micrographs after immersion of the inhibitors in the corrosive media except polishing lines proving that the metal surface is homogeneously covered with the inhibitor molecules.

The formation of protective film of inhibitors on mild steel surface was also supported by EDS analysis. The EDS examination on mild steel surface was performed in the uninhibited and inhibited 1M H_2SO_4. The percentage atomic content of MS samples obtained from EDS analysis is listed in Table 6.12. Fig. 6.28 represent the EDS spectrum of uninhibited mild steel specimen, the peak of oxygen is absent which confirms the dissolution of air-formed oxide film and free corrosion of bare metal. However, for inhibited solutions Figs. 6.29 and 6.30, the EDS spectra showed additional lines

characteristic of N and S (due to the N and S atoms of the inhibitors). From the spectra of DTPT and BPPT it is evident that the Fe peaks are significantly suppressed in the inhibited sample relative to the uninhibited mild steel sample indicating that the corrosion process is hindered by adsorption of the inhibitors on the mild steel surface. This behavior can be ascribed to the formation of a protective layer consisting of an organic thin film and a small amount of Fe compound.

6.3.3.3 X-ray diffraction patterns

The XRD patterns of the corrosion products give qualitative information about the possible phase present. The patterns obtained clearly reveal the presence of metal and metal oxide phases. The XRD results are presented in Figs. 6.31 & 6.32. Peaks at 2θ = 29.8, 35.3 and 64.5° can be assigned to oxides of iron. Thus, surface of the metal immersed in 1M H_2SO_4 (blank) contains iron oxides, which are most probably Fe_3O_4 and FeOOH as shown in Fig. 6.31 (Blank). The XRD pattern for the metal immersed in 1M H_2SO_4 containing optimum concentrations of the inhibitors (DTPT) are given in Fig. 6.32. The intensity of the peaks due to oxides of iron such as Fe_3O_4 and FeOOH are found to be very low and the peaks due to iron alone observed at 2θ = 44.3, 65 and 82.4° are very high, confirming the presence of inhibitor molecule on the metal surface.

6.3.3.4 Atomic force microscopy

In order to establish whether inhibition is due to the formation of a film on the metal surface through adsorption, atomic force micrographs of the mild steel plates were recorded. Surface roughness analysis for mild steel specimen immersed in 1M H_2SO_4 for a period of 3 hours in uninhibited and inhibited solution was studied using atomic force microscopy. The two-dimensional and three dimensional AFM images of uninhibited and inhibited mild steel samples are shown in Figs. 6.33 & 6.34. The average roughness of mild steel plate immersed in 1M H_2SO_4 was found as 145.705 nm. It is clearly shown in Fig. 6.33 that mild steel sample is badly damaged due to the acid attack on the surface. However, in the presence of optimum concentration (1 mM) of DTPT the average roughness was reduced to 32.51 nm as shown in Fig. 6.34. The lower value of roughness for DTPT clearly reveals that the surface is more homogeneous and confirms the formation of the protective film on the metal surface[42, 43].

6.3.4 Quantum chemical studies

6.3.4.1 Quantum chemical study of non-protonated form of the studied inhibitors in aqueous phase

Table 6.13 (a) and 6.13 (b) shows values of some quantum chemical parameters computed for selected heterocyclic bis-compounds namely thiophene derivatives (DTPT, DTPH), pyridine derivatives (BPPT, BPPH) and benzene derivatives (BPT, BPH). Molecular properties of the studied bis-derivatives provide information on the reactivity and selectivity of the compounds, such information is useful in the comparison of the trends in reactivity among different compounds and indeed, it is important to understand the interaction of the inhibitor with the metal surface. The selected bis-derivatives of thiophene, pyridine and benzene derivatives followed the experimental inhibition efficiency with respect to quantum chemical parameters E_{LUMO} and softness whereas other parameters such as E_{HOMO}, ΔN and energy gap does not correlate well with the experimental inhibition efficiency. In non-protonated form, some quantum chemical parameters do not show correlation with the experimental order, therefore it is necessary to study the influence of protonation for the selected bis-derivatives.

6.3.4.2 Quantum chemical study of protonated form of the studied inhibitors in aqueous phase

In acidic environment the inhibitors also interact with the acidic solution leading to the possibility of co-existence of both protonated and non-protonated species of the inhibitor. In such cases, it is interesting to investigate the preferred species to interact with the metal surface, to study the influence of protonation on the molecular structures and the molecular properties of the inhibitors. The possible sites for protonation are the heteroatoms present in each compound. The results of the calculation on the different possible sites for protonation show that the preferred site for protonation is N17, N24 for (DTPT), N17, N20 for (BPPT, BPT) and N12, N24 for (DTPH, BPPH and BPH). This is the site that is less sterically hindered because there are no other protons present. Moreover, it is the only position that is common to all the selected compounds, making it easy to compare the effects of protonation across structures.

Accoding to the frontier molecular orbital theory, the energy of the highest occupied molecular orbital (E_{HOMO}) and that of the lowest unoccupied molecular orbital

(E_{LUMO}) are important indices for predicting the reactivity of a chemical species. Therefore, increasing values of E_{HOMO} will facilitate the adsorption of the inhibitor and ensure better inhibition efficiency by improving the transport process through the adsorbed layer. On the other hand decreasing values of E_{LUMO} indicates the ability of a molecule to accept an electron. The difference between E_{LUMO} and $E_{HOMO,}$ *i.e.,* the energy gap (ΔE) is another index that has been found to have excellent correlations with experimental inhibition efficiencies. The energy gap is related to the hardness and softness of the molecule. Soft molecules are more reactive than hard molecules because the energy to remove electron from the last occupied orbital will be low[44]. Table 6.16 (a) and 6.16 (b) shows the quantum chemical parameter for the selected inhibitors in protonated form. From the Table 6.16 (a) and 6.16 (b), it is clear that increasing values of E_{HOMO}, softness and ΔN follows the trend DTPT > DTPH; BPPT > BPPH and BPT > BPH and the decreasing values of E_{LUMO}, hardness and the energy gap (ΔE) follows the order DTPT < DTPH; BPPT < BPPH and BPT < BPH. This trend is consistent with experimental data.

6.3.4.3 Mulliken charge density distribution

The atomic charges of the studied bis-derivatives obtained by Mulliken's population analysis in both non-protonated and protonated forms are shown in Table 6.14 (a), 6.14 (b), 6.17 (a) and 6.17 (b). These charges indicate that there is more than one active centre and it is confirmed that, the more negative the atomic partial charges of the adsorbed centre, the more easily the atoms donate its electron to the unoccupied d-orbital of the metal[45-47]. The atomic charges in Table 6.14 (a), 6.14 (b), 6.17 (a) and 6.17 (b) shows that N and O atoms have high negative charges whereas the S atom bears positive charge for the inhibitors (DTPT, BPPT and BPT). Hence N and O atoms are the most probable centres of adsorption *via.,* the lone pair of electrons in the studied molecules. Moreover, it is evident from Mulliken analysis that the mechanism of adsorption between the bis-derivatives and mild steel surface occurs mainly through the N and O atoms and not the sulphur atom. The optimized structures, HOMO and LUMO orbitals of bis-derivatives in non-protonated and protonated forms are presented in Table 6.15 and 6.18 and it reveals that LUMO and HOMO densities are distributed over the entire molecule.

6.3.5 Mechanism of corrosion inhibition and evaluation of inhibitors

From the results of different electrochemical and weight loss measurements, it has been concluded that all the synthesized bis-derivatives inhibit the corrosion of mild steel in 1M H_2SO_4 by adsorption process[48, 49]. It is reported[50] that the strength of adsorption is affected by number of adsorption sites, charge density, molecular size and mode of interactions with the metal surface and the stability of the film to be formed. Here, the adsorption of the inhibitor compounds on the mild steel surface could occur directly on the basis of donor-acceptor behaviour between the lone pair of heteroatoms and the extensively delocalized π-electrons of the inhibitor molecules and the vacant d-orbital of the iron surface atoms[51]. These bis-derivatives are able to get adsorbed on anodic sites through N, O & S atoms, heterocyclic rings and aromatic rings which are electron donating groups. Thus, adsorption of these bis-derivatives on the steel surface decreases its anodic reaction by blocking the active sites and therefore decreases the anodic dissolution of mild steel. Generally corrosion takes place through the following two reactions

(a) Anodic reaction which leads to metal dissolution

$$M \longrightarrow M_n^+ + ne^- \longrightarrow 6.16$$

(b) Cathodic reaction which results in hydrogen evolution in acid media

$$2H^+ + 2e^- \longrightarrow H_2 \longrightarrow 6.17$$

According to the polarization results, bis-derivatives followed mixed inhibition mechanism. Some of the organic molecules in bis-derivatives get protonated and these cationic forms may adsorb directly on the cathodic sites of the mild steel and reduce the hydrogen evolution reaction. On the other hand, these derivatives may adsorb on anodic sites of mild steel through the π-electrons of the aromatic rings and lone pair of electrons on the heteroatoms and thereby inhibit the anodic dissolution of mild steel. Hence by following the above mechanism, bis-derivatives showed mixed type of inhibition on mild steel surface in 1M H_2SO_4.

The inhibitors taken for study can be grouped into 3 classes of derivatives namely thiophene, pyridine and benzene. Among the 3 classes the order of inhibition efficiency is

Thiophene derivatives: DTPT > DTPH > DTPP > DTPO

Pyridine derivatives: BPPT > BPPH > BPPP > BPPO

Benzene derivatives: BPT > BPH > BPP > BPO

In all the 3 classes of compounds, the same trend in inhibition efficiency is observed *i.e.*, pyrimidine with SH group > pyrimidine with OH group > pyrazole > oxazole.

All the bis derivatives have almost the same size but differ in the substituent groups. In all the three classes of compounds, the compounds with pyrimidine nucleus with –SH group exhibit maximum inhibition efficiency of 99.03%, 93.05 % and 84.02 % respectively. Next in the sequence are the compounds with pyrazole and oxazole moieties. The best performance of compounds with pyrimidine nucleus can be attributed to the presence of electron releasing –SH and –OH groups which increases the π-electron density on the phenyl ring. Presence of heterocyclic rings with –NH-N=C< in the pyrazole moiety and –O-N=C< in the oxazole moiety are also responsible for adsorption of the inhibitors on the metal surface.

Out of the three classes of compounds, the thiophene derivatives exhibited maximum inhibition efficiency. The thiophene ring with two electron donating $–CH_3$ groups are responsible for the higher adsorption. The $–CH_3$ group has a positive mesomeric effect (+M) and a positive inductive effect (+I) which increases the electron density on the thiophene rings and increase the adsorption of these derivatives to a greater extent on the metal surface. Since –SH is better electron releasing group as compared to –OH group, hence it facilitates greater adsorption of –SH substituted derivatives on the mild steel surface than hydroxy substituted ones. This leads to higher inhibition efficiency of DTPT, BPPT, BPT than DTPH, BPPH, BPH.

6.4 CONCLUSIONS

The results and discussion arrived based on the investigations of bis-pyrimidine, bis- pyrazole and bis-isooxazole derivatives are

- Three classes of derivatives namely benzene, pyridine and thiophene containing bis pyrimidine, pyrazole and oxazole nucleus have been synthesized and used as corrosion inhibitors for mild steel in 1M H_2SO_4 medium.
- Among the three classes, the order of inhibition efficiency are as follows
  Thiophene derivatives: DTPT > DTPH > DTPP > DTPO
  Pyridine derivatives: BPPT > BPPH > BPPP > BPPO
  Benzene derivatives: BPT > BPH > BPP > BPO
- In all the three classes of compounds, the compounds with pyrimidine nucleus with –SH group exhibit maximum inhibition efficiency of 99.03 %, 93.05 % and 84.02 %.
- The results of weight loss and electrochemical measurements show that all the three classes of compounds have an excellent inhibiting property for acidic corrosion of mild steel.
- In addition even a very small amount of bis-derivatives to the acid solution retards the corrosion rate of the metal and the extent of retardation is concentration and temperature dependent. This is generally attributed to the increase in the number of adsorption sites which allow higher inhibition.
- The synthesized bis-compounds obey Langmuir adsorption isotherm.
- Potentiodynamic polarization measurements proved the mixed nature of the inhibitors however the minor shift of E_{corr} values towards positive direction suggests the predominant anodic control over the reaction.
- The results obtained from different techniques are in good agreement with each other.
- The results from FTIR, SEM-EDS, AFM and XRD studies confirmed the formation of the protective film on the metal surface.

6.5 REFERENCES

1. I. Jarak, M. Kralj, I. Piantanida, L. Suman, M. Zinic, K. Pavelic, G. Karminski-Zamola, Bioorg. Med. Chem., **14** (2006) 2859.
2. D. Peters, A.B. Hornfeldt, S. Gronowitz, J.Heterocycl. Chem., **27** (1990) 2165.
3. S. Kukolja, S.E. Draheim, B.J. Graves, D.C. Hunden, J.L. Pfeil, R.D.G. Cooper, J.L. Ott,J. Med. Chem., **28** (1985) 1896.
4. J.D. Prugh, G.D. Hartman, P.J.; Mallorga, B.M. McKeever, S.R. Michelson, M.A. Murcko, H. Schwam, R.L. Smith, J.M. Sondey, J.P. Springer, M.F. Surgrue, J. Med.Chem., **34** (1991) 1805.
5. M.S. Egbertson, J.J. Cook, B. Bednar, J.D. Prugh, R.A. Bednar, S.L. Gaul, R.J. Gould, G.D. Hartman, C.F. Homnick, M.A. Holahan, L.A. Libby, J.J. Jr Lynch , R.J. Lynch, G.R. Sitko, M.T. Stranieri, L.M. Vassallo, J. Med. Chem., **42** (1999), 2409.
6. A. Popova, M. Christov, S. Raicheva, E. Sokolova, Corros. Sci., **46** (2004) 1333.
7. A.M. Asiri, H.M. Marwani, K.A. Alamry, M.S. Al-Amoudi, S.A. Khan, S.A. El-Daly, Int. J. Electrochem. Sci., **9** (2014) 799.
8. A.F. Abbas, A.A. Turki, A. Jameel Hameed, J. Mater. Environ. Sci., **3** (2012) 1071.
9. J.O.M. Bockris, D. Drazic, Electrochim. Acta., **7** (1962) 293.
10. E.E. Oguzie, Mater. Chem. Phys., **87** (2004) 212.
11. E.E. Oguzie, G. Onuoha, A.I. Onuchukwu, Mater. Chem. Phys., **89** (2005) 305.
12. A.U. Ezeoke, O.G. Adeyemi, O.A. Akerele, N.O. Obi-Egbedi, Int. J. Electrochem. Sci., **7** (2012) 533.
13. B. Bonnelly, T.C. Dowine, R. Grzekowiak, H.R. Hamburg, D. Short, Corros. Sci., **18** (1978) 109.
14. A. Chetouani, B. Hammouti, A. Aouniti, N. Benchat, T. Benhadda, Prog. Org. Coat., **45** (2002) 373.
15. "Corrosion control" NAVFAC MO-307 September 1992.
16. O. Olivares, N.V. Likhanova, B. Gomez, J. Navearreie, M.E. Llanoserrano, E. Arce, J.M. Hallen, Appl. Surf. Sci., **252** (2006) 2894.
17. C.S. Venkatachalam, S.R. Rajagopalan, M.V.C. Sastry, Electrochimica. Acta., **26** (1981) 1219.

18. A.A. Khadom, A.S. Yaro, A.S. Altaie, A.A.H. Kadum, Portugaliae Electrochimica Acta., **27** (2009) 699.
19. K.F. Khaled, K.B. Samardzija, N. Hackerman, J. Appl. Electrochem., **34** (2004) 697.
20. E.A. Noor, Int. J. Electrochem. Sci., **2** (2007) 996.
21. M. Lebrini, F. Robert, C.Roos, Int. J. Electrochem. Sci., **5** (2010) 1698.
22. X. Wang, H. Yang, F. Wang, Corros.Sci., **53** (2011) 113.
23. E.A. Noor, J. Electrochem., **39** (2009) 1465.
24. M.A. Amin, J. Appl. Electrochem., **36** (2006) 215.
25. H. Ashassi-Sorkhabi, B. Shaabani, D. Seifzadeh, Electrochim.Acta, **50** (2005) 3446.
26. W. Durnie, R. De Marco, B. Kinsella, A. Jefferson, J. Electrochem. Soc., **146**, (1999) 1751.
27. T.P. Zhao, G.N. Mu, Corros. Sci., **41** (1999) 1937.
28. A.K. Singh, S.K. Shukla, M. Singh, M.A. Quraishi, Mater. Chem. Phys., **129** (2011) 68.
29. V. Branzoi, F. Branzoi M. Bai barac, Mater. Chem. Phys., **65** (2000) 288.
30. S. Issaadi, T. Douadi, A. Zouaoui, S. Chafaa, M. A. Khan, G. Bouet, Corros. Sci., **53** (2011) 1484.
31. H. Shih, H. Mansfeld, Corros. Sci., **29** (1989) 1235.
32. M. Elayyachy, A. El Idrissi, B. Hammouti, Corros. Sci., **48** (2006) 2470.
33. K.S. Jacob, G. Parameswaran, Corros. Sci., **52** (2010) 224.
34. I. Ahamad, R. Prasad, M.A. Quraishi, Corros. Sci., **52 (**2010) 933.
35. K.F. Khaled, Electrochimca. Acta., **53** (2008) 3484.
36. K. Adardour, O. Kassou, R. Touir, M. Ebn Touhami, H. Elkafsaoui, H. Benzeid, E.M. Essassi, M. Sfaira, J. Mater. Environ. Sci., **1 (2)** (2010) 129.
37. K.C. Pillai, R. Narayan, Corros. Sci., **23** (1983) 151.
38. A.K. Vijh, B.E. Conway, Chem. Rev., **67** (1967) 623.
39. H.A. Sorkhabi, M.R. Majidi, K. Seyyedi, Appl. Surf. Sci., **225** (2004) 176.
40. M.A. Amin, K.F. Khaled, Corros.Sci, **52** (2010) 1762.
41. S.S. Abe El Rehim, S. Refaey, F. Taha, M.B. Saleh, R.A. Ahmed, J. Appl. Electrochem., **31** (2001) 429.
42. M. Mobin, S. Masroor, Int. J. Electrochem., **7** (2012) 6920.

43. M. Hakeem, S. Rajendran, A.P.P. Regis, J. Engg. Comp. Appl. Sci., **3** (2014) 1.
44. F. Bentiss, M. Traisnel, N. Chaibi, B. Mernari, H. Vezin, M. Lagrenee, Corros. Sci., **44** (2002) 2271.
45. K.F. Khaled, Electrochim. Acta., **53** (2008) 3484.
46. K.F. Khaled, M.A. Amin, J. Appl. Electrochem., **38** (2008) 1609.
47. J.M. Roque, T. Pandiyan, J. Cruz, E. Gracia-Ochoa, Corros. Sci., **50** (2008) 624.
48. K.M. Govindaraju, D. Gopi, L. Kavitha, J. Appl. Electrochem., **39** (2009) 2345.
49. D. Schweinsgberg, G. George, A. Nanayakkawa, D. Steinert, Corros. Sci., **28** (1988) 33.
50. A. Fouda, M. Moussa, F. Taha, I. Neena, Corros.Sci., **26** (1986) 719.
51. S. Muralidharan, M.A. Quarishi, S.V.K. Iyer, Corros.Sci., **37** (1995) 1739.